Generation of localized lower-hybrid current drive by temperature perturbations

S.J. Frank[1], A.H. Reiman[2], N.J. Fisch[2] and P.T. Bonoli[1]

[1] Massachusetts Institute of Technology: Plasma Science and Fusion Center, Cambridge, Massachusetts 02139, United States of America
[2] Princeton Plasma Physics Laboratory, Princeton, New Jersey 08544, United States of America

E-mail: sfrnk@mit.edu

CrossMark

Abstract
Despite high demonstrated efficiency, lower-hybrid current drive (LHCD) has not been considered localized enough for neoclassical tearing mode (NTM) stabilization in tokamaks. This assessment must be reconsidered in view of the radiofrequency current condensation effect. We show that an island with a central hot spot induces significant localization of LHCD. Furthermore, in steady state tokamaks where a significant amount of current is provided by LHCD, passive stabilization of NTMs may occur automatically, particularly as islands become large, without requiring precise aiming of the wave power.

Some figures may appear in colour only in the online journal

1. Introduction

Disruptions are a major concern in for ITER and future tokamak reactors. One way to address disruptions is through mitigation, i.e. minimizing damage caused by disruptions. Yet disruption mitigation will not alone suffice for dealing with disruptions. Every mitigated disruption in a reactor class device will cause some damage to the first wall, and it is estimated that ITER will need to maintain a disruption rate of less than 1% to keep cumulative damage to the first wall at an acceptable level. In fusion reactors, unplanned shutdowns will severely impact commercial viability, even if mitigation is 100% successful, and disruptions will need to be extremely rare. Every mitigated disruption will also carry with it some level of risk. It will be desirable to avoid disruptions to the extent possible. The Joint European Torus (JET) device has had a 16% rate of unintended disruptions since it was converted to have an ITER-like wall and 95% of the disruptions are preceded by the appearance of large locked islands [1]. A statistical analysis of disruptions in JET found that there is a distinct island width at which islands cause the tokamak to disrupt corresponding to approximately 30% of the minor radius [2]. This suggests that islands are playing a key role in triggering disruptions. Thus, there is then a critical need for a capability to suppress magnetic islands in tokamaks before they can cause disruptions.

The stabilization of magnetic islands by noninductive RF-driven current has long been predicted [3]. Particularly attention has been given to electron cyclotron current drive (ECCD) [4] and significant progress has been made using this approach, both theoretical [5, 6] and experimental [7]. The question remains, however, what is the best means of noninductive RF-driven current to stabilize these islands? There are many RF waves that might be employed to generate toroidal current in tokamaks [8]. The waves that have received the most attention have been the lower hybrid wave for lower hybrid current drive (LHCD) [9] and the electron cyclotron wave for ECCD [4]. Both of these waves have been employed to generate substantial noninductive toroidal current for the purpose of operating tokamaks in the steady state. In this regard, LHCD has been shown to be particularly efficient with the theoretical efficiency well supported by detailed comparison to experiments

[10]. On the other hand, for the purpose of neoclassical tearing mode (NTM) stabilization, while LHCD has received some experimental attention [11], nearly all of experimental effort to date has been focused on ECCD. ECCD has been preferred since it is thought to be the only current drive method that can operate in 'in a highly localized, robustly controllable way' [12].

However, the recently identified RF current condensation effect causes RF wave power deposition, that is initially broad, to condense near the center of a magnetic island at high power [13]. This effect relies upon positive feedback; the damping of the power in a magnetic island raises the temperature at the island center relative to the temperature of its edge. For waves with damping rates sensitive to the temperature the wave damping is then increased at the island center. Increased damping at the island center further raises the central island temperature relative to the periphery. The current drive profile then follows the power deposition profile. This effect is pronounced for both LHCD and ECCD, as both of these RF heating and current drive methods have damping which is extremely sensitive to the electron temperature [14, 15]. However, since LHCD normally has both a broader profile and greater temperature sensitivity than ECCD, the current condensation effect should provide relatively greater benefits. Thus, the assessment that LHCD might be too broad for NTM stabilization must be reconsidered in view of the RF current condensation effect.

To perform this assessment, we evaluate the sensitivity of lower hybrid (LH) power deposition to a temperature perturbation, and the extent to which an elevated central island temperature can localize the damping of lower hybrid waves. The evaluation is carried out by considering lower hybrid waves launched into a model ITER equilibrium, with an assumed temperature perturbation near a rational magnetic surface where islands might form. The ITER equilibrium was chosen as a canonical example of a reactor relevant equilibrium susceptible to 2–1 and 3–2 magnetic islands. What we show is that, for lower hybrid waves launched from the high-field side of the tokamak ('inside launch'), there can be substantial current drive localization for temperature perturbations as large at 15% in even moderately large islands.

Although we report on only a partial scan of all possible parameters, what can already be deduced from the scenarios offered is that, while the LHCD profile remains broader than scenarios offered by ECCD, the localization by the temperature perturbation is clear and pronounced. What this suggests is that a relatively broad profile of LHCD, which might be employed for supplying a significant part of the current in steady state reactors, could act as a passive methodology for controlling the NTM. Passive stabilization stands in contrast to needing to accurately determine the location of the island and then to direct the RF power as needed for ECCD stabilization. In other words, in the presence of broad deposition of LHCD, an emerging island will automatically develop a hot center and condense the lower hybrid driven current so as to passively stabilize the island. In the case of passive stabilization, much of the RF power is not used for the stabilization but might be used for maintaining a steady state. However, a higher degree of localization may be possible when a launcher specifically designed to maximize the effect is used.

The paper is organized as follows: in section 2, we discuss properties of the lower hybrid wave and how it triggers the RF condensation effect. In section 3, we show with raytracing/Fokker-Planck simulations that the damping in the presence of a temperature perturbation can lead to significantly enhanced power deposition near the local temperature maximum. In section 4, we evaluate the importance of non-Maxwellian effects on the localization of LHCD and RF condensation. In section 5, we summarize our main conclusions.

2. Lower hybrid waves

Lower hybrid current drive has long been employed as an efficient means of current drive and non-inductive sustainment of tokamak discharges. LH waves have frequencies corresponding to the lower-hybrid limit, $\Omega_i \ll \omega \ll \Omega_e$. Here ω is the angular frequency of the lower-hybrid waves and Ω_i and Ω_e are the ion and electron cyclotron gyro-frequencies respectively. The lower-hybrid limit typically corresponds to 1–10 GHz frequency window over a wide range of tokamak parameters. Lower hybrid waves are launched from a waveguide with a slow-wave launching structure which is placed close to the plasma edge in order to ensure good coupling as the lower-hybrid wave is evanescent unless its frequency is below the electron plasma frequency, ω_{pe} [16]. The waves then propagate until they encounter one of two limits. The first limit, corresponding to LH slow-wave accessibility, is [17, 18]:

$$n_{||} \geq n_{||acc} = \frac{\omega_{pe}}{\Omega_e} + \sqrt{1 + \left(\frac{\omega_{pe}}{\Omega_e}\right)^2 - \left(\frac{\omega_{pi}}{\Omega}\right)^2} \qquad (1)$$

where $n_{||}$ is the parallel refractive index corresponding to $ck_{||}/\omega$ and ω_{pi} is the ion plasma frequency. When the parallel refractive index drops below this limit the wave is reflected and mode converted into a fast wave. The other limit on LH wave propagation is the onset of Landau damping when [17–19]:

$$n_{||} \geq \frac{5.4}{[T_e\,(keV)]^{1/2}} \qquad (2)$$

When this relation is satisfied the wave is quickly absorbed by non-thermal electron Landau damping at three to six times the electron thermal velocity, v_{the} [19] and drives a plasma current there [5, 10]. The non-thermal nature of LH wave damping causes significant distortion of the electron distribution function at high electron energies necessitating a Fokker-Planck calculation to determine the non-linear evolution of the distribution function in response to LHCD and predict the LH wave's absorption and the current drive profiles.

In previous studies of reactor relevant parameter regimes simulations of LHCD have indicated that the current drive profiles should be broad and off axis, between r/a ∼ 0.6–0.8 [20–27], in comparison to the localized current drive which

can be obtained with electron-cyclotron current drive (ECCD) [12, 28, 29]. While LHCD has been suggested as a mechanism for NTM suppression in future tokamak designs no mechanism by which the LHCD could be localized to effectively stabilize the NTMs was described [21, 22]. The temperature perturbation associated with thermal insulation in a magnetic island [30–36], however, can be large enough to induce significant localization of the LH wave. Moreover, due to the shape of the temperature perturbation present in these islands, wave damping and therefore current drive is localized near the O-point of the island where the temperature is peaked and the current drive is most effective at suppressing the island [3].

Lower hybrid current drive localization can occur because of the non-thermal nature of LH wave damping. A small increase in electron temperature can increase the number of electrons with $v_e = v_{ph,LH}$ (the phase velocity of the LH wave), by many orders of magnitude inducing strong wave damping, a consequence of the nonthermal electron population available for damping $\propto e^{-\left(\frac{v_{ph,LH}}{v_{the}}\right)^2}$. As a result of the localization, and thus increased heating and current drive within the island, further wave localization can occur as a result of RF-condensation, which is, a non-linear feedback effect that occurs as a result of the RF power deposition balancing with the thermal diffusion [13]:

$$\nabla \cdot [n_e \kappa \cdot \nabla T(x)] = -[P_{rf}(T(x)) + P_{OH}(T(x))] \quad (3)$$

where T is the temperature, n_e is the electron density, κ is the thermal diffusivity, P_{rf} is the RF heating power, P_{OH} is the ohmic heating power, and $\mathbf{x}$ is the spatial coordinate. The evolution of equation (3) leads to further peaking of the island temperature profiles about the O-point. The temperature peaking in turn increases LH wave damping, P_{rf}, at the island's O-point leading to a feedback loop. This is the RF condensation effect which can be used to further localize LHCD at an island's O-point and greatly increase LHCD's efficiency when used to suppress magnetic islands.

3. Simulations of LHCD localization

Simulations of LHCD were performed using the GENRAY (General Raytracing) raytracing code [37] and the plasma distribution function's response to the LH wave absorption was modeled using the CQL3D (Collisional/Quasilinear 3D) Fokker-Planck code [38, 39]. GENRAY models the propagation and absorption of LH waves in the Wentzel-Kramers-Brillouin approximation using raytracing/geometric optics and passes the resulting ray paths to the CQL3D Fokker-Planck code. CQL3D reconstructs the quasi-linear diffusion coefficient along the ray paths then quasi-linearly evolves the distribution function in time and recalculates the damping along the rays. After a sufficient number of timesteps in CQL3D the ray absorption and perturbed distribution function reach a steady state that correctly models the ray damping on a perturbed distribution function. GENRAY/CQL3D provide ray data that can be analyzed on a ray-by-ray basis and current drive profiles that can be used later for stability calculations

in order to predict the required launched LH power needed to suppress a magnetic island.

We have calculated how imposed temperature perturbations affect LH power deposition. In practice we are interested in local temperature perturbations produced by the presence of magnetic islands, with their associated change in topology and associated boundary conditions. For our purposes here, of establishing the sensitivity of the power deposition to the temperature perturbation and the associated localization of the power deposition, it is sufficient to consider only temperature perturbations. The coupled problem, with the nonlinear feedback between the temperature perturbation and the power deposition described by equation (3), has been left to future work. In order to properly calculate the RF power source term in equation (3), the magnetic island's geometry will need to be considered rigorously in the raytracing and Fokker-Planck simulations.

In the following simulations the magnetic equilibrium, temperature profiles, and density profiles, of ITER Scenario 2 [40] generated using TRANSP [41] were used to model LHCD localization. Scenario 2 was chosen as a canonical example of a reactor relevant parameter space susceptible to 2–1 and 3–2 magnetic islands [42]. The temperature, density, and safety factor profiles used in the simulations appear in figure 1. The ITER scenarios, unlike many other reactor relevant scenarios, are highly vetted, and ITER Scenario 2 has q = 2 and q = 1.5 surfaces that are far enough off-axis that they are accessible to LH waves. ITER scenario 2 also has high, reactor-relevant, electron core temperature, T_{e0}, ensuring that the LH wave damps in a single pass. The strong single pass damping of the LH waves in this discharge ensures that the raytracing simulations stay far from the regimes where reflections and edge cut-offs can occur causing the Wentzel–Kramers–Brillouin (WKB) approximation to break down. Additionally, in strong damping regimes, the LH wave is localized to so called 'resonance cones' that propagate in an organized fashion [43] as opposed to weakly damped regimes where the wave exhibits a cavity mode like propagation pattern filling the tokamak stochastically [44, 45]. An example of the propagation of the LH waves in Scenario 2 is shown in figure 2. As LH wave propagation is predictable in strong damping, one can more easily extrapolate the localization associated with a one-dimensional temperature perturbation to the localization that would occur in a more realistic three-dimensional island geometry. This allows one to make an accurate assessment of the LHCD localization expected in a more complex geometry as the wave absorption in the one-dimensional case will be similar to the three-dimensional case assuming the waves hits the island relatively close to the island midplane.

The evolution of the magnetic island may be neglected in these analyses using a timescale argument. The energy confinement time of the magnetic island is short compared to the global resistive timescale, on the order of seconds in ITER, on which the island is growing and this ordering is already used in the original analysis of the RF condensation effect [13]. The quasi-linear timescale, corresponding to the RF response to and the evolution of the plasma distribution function, on which this analysis is performed reaches a steady state in < 10 ms.
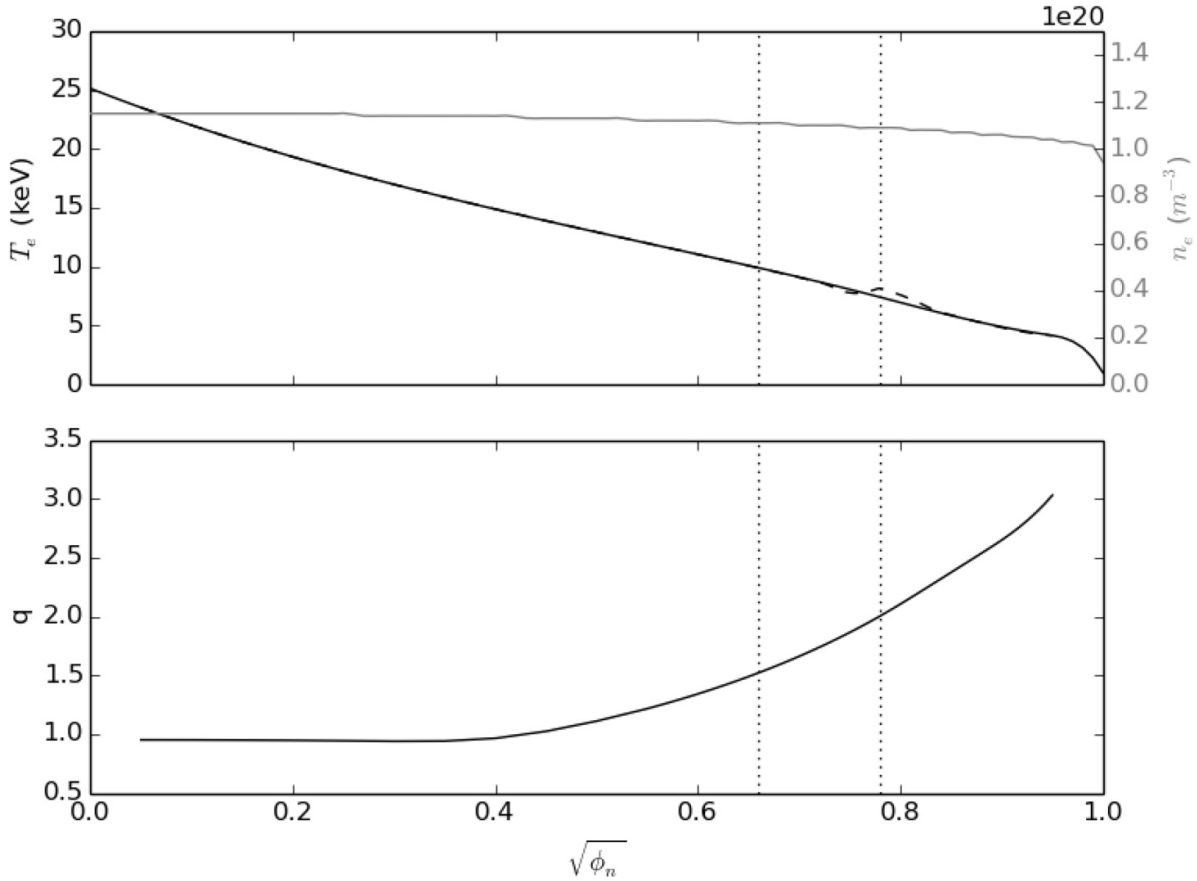
Figure 1. ITER Scenario 2 temperature (T_e), electron density (n_e), and safety factor profiles (q) vs the square root of the normalized toroidal magnetic flux (ϕ_n). The profiles and magnetic equilibrium were generated using TRANSP [39] and the electron temperatures were then perturbed with a perturbation of the form in equation (6) about the q = 2 or q = 1.5 flux surfaces. An example of a perturbation at the q = 2 surface with w = 20 cm and δT = 0.10 is shown by the dashed line in the upper plot.

This is a shorter timescale than the other relevant timescales in the RF condensation problem in ITER. The timescale separation allows us to decouple the problem of RF sensitivity to island temperature perturbations from the island evolution and the RF condensation effect in the analysis here.

The magnetic field perturbation δB from the magnetic island is also not included in these simulations, but it is expected to have little effect on LH wave propagation. The width of a magnetic island is approximately:

$$W \approx 4\sqrt{\frac{r\delta B}{smB_p}} \tag{4}$$

where: δB is the resonant component of the radial field, $s = q'/q$, m is the mode number of the perturbation, and B_p is the poloidal magnetic field. For a 2–1 island this equation becomes:

$$\frac{\delta B}{B} \approx \frac{1}{32}\frac{a}{R}\frac{W^2}{a^2} \tag{5}$$

In the case of a 20 cm q = 2 island in ITER Scenario 2 the predicted $\delta B/B_0$ is $\sim 1 \times 10^{-4}$ [46]. For a perturbation of this magnitude it can be shown that no element of the dielectric tensor in the LH limit [18] is modified by a value greater

than $\sim 0.1\%$. Since the LH wave is strongly damped, only a single pass through the perturbation will occur, and any additive effects from multiple interactions, which could make a small perturbation more significant, can be ignored. Thus, we expect that the effect of δB perturbation on wave propagation can be safely ignored in our study of the LH wave sensitivity to island temperature perturbations here. Previous studies examining the LH wave response to perturbations in the background magnetic field B_0 serve to reinforce the validity of this assumption [47].

The δB perturbation from the magnetic island, while is expected to be unimportant to wave propagation, may be more important in the FP calculation. The θ−(poloidal) axisymmetry along a flux surface, assumed in CQL3D, is broken when a magnetic island forms. As solving the FP equation with RF diffusion in a magnetic geometry without θ symmetry would require the creation of a novel code, or at the very least would necessitate significant modifications to an existing code, we have opted to minimize error in our simulations here by ensuring that the LH wave is strongly single pass damped. If the wave were to pass through the perturbation many times at many different θ locations, as is the case in a weakly damped discharge, a significant error could result in not including the θ variation. However, as the wave only passes through a given flux surface a single time at a single θ location
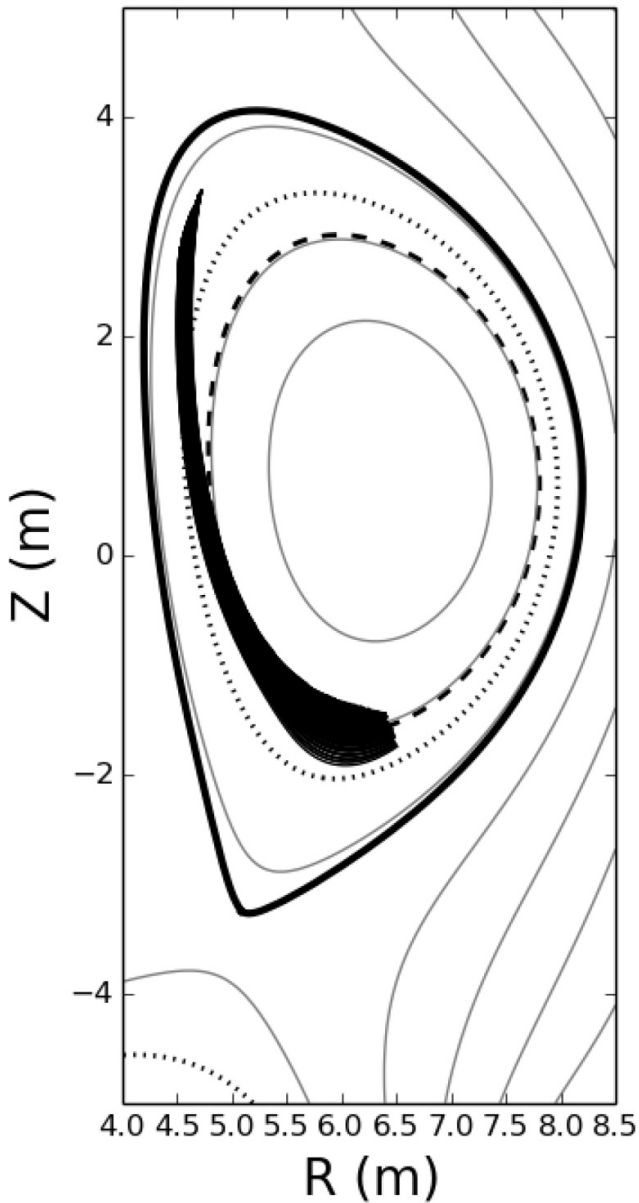
Figure 2. Two-dimensional projection of ray paths in an ITER Scenario 2 simulation with no temperature perturbation. The rays shown as bold black lines, propagate in an orderly, predictable, fashion characteristic of strong damping. Rays are launched slightly inside the last closed flux surface at r/a = 0.98. The dotted line indicates the q = 2 surface and the dashed line indicates the q = 1.5 flux surface.

condensation feedback is included and will be discussed further in section 4 where non-Maxwellian effects are considered.

The one-dimensional radial temperature perturbation used in these simulations has the form:

$$T = T_0 \left[1 + \delta T \left(\frac{\rho}{w/2}\right)^2 + \delta T \sin\left(\frac{2\pi\rho}{w/2}\right)\right], -\frac{w}{2} \leq \rho \leq 0$$

$$T = T_0 \left[1 + \delta T \left(\frac{\rho}{w/2}\right)^2\right], 0 < \rho \leq \frac{w}{2} \quad (6)$$

$$T = T_0, otherwise$$

where w corresponds to the island width, ρ corresponds to a relative radial coordinate in the magnetic island extending from -w/2 to w/2, and δT corresponds to a free parameter that allows us to set the perturbation size. The temperature perturbation was centered about either the q = 2 or q = 1.5 flux surfaces. The perturbation in figure 1, resulting from equation (6), is qualitatively similar to the radial temperature perturbations induced by magnetic islands without the presence of local RF heating in previous tokamak experiments, with maximum δT values of ~ 0.05–0.15, as measured using electron-cyclotron emission diagnostics [30–32, 34, 46]. In future studies where realistic island geometry is added the temperature perturbation would be directly calculated from equation (3). The width of the island, w, was set to either 10 cm or 20 cm and the δT value associated with the perturbation was varied between 0.05 and 0.15 in steps of 0.05.

In order to ensure LH wave accessibility to the 3/2 and 2/1 rational surfaces it was necessary to launch the LH waves from the high-field side (HFS) of the Scenario 2 discharge. This is *not* a realistic launcher configuration for ITER as there is not port space for the installation of a LHCD launcher on HFS or room to run the RF waveguides to such a launcher even if space were available. However, it is relevant to other future reactor design studies with similar parameters such as pulsed or hybrid scenarios in ARC (Affordable Robust Compact) class devices, EU-DEMO, and Chinese Fusion Engineering Test Reactor (CFETR) [24, 25, 48]. Investigation of this concept in ITER rather than one of these reactor concepts where HFS launch is possible was done as the ITER Scenario 2 has seen substantially more development and physics validation than any other reactor relevant scenarios and any important results derived from it can be translated to these other devices with high confidence. The HFS launch was required because the high density and temperature pedestal in Scenario 2 causes the LH wave accessibility window defined by equations (1) and (2) to be very small. The maximum accessible $n_{||}$ value at the low-field side (LFS) midplane for ITER Scenario 2 is defined by equation (1) to be $\sim$-2.0 significantly lower than ITER Scenario 4 where an $n_{||} = -1.8$ may be launched from the LFS as the pedestal density is $\sim 7 \times 10^{19}$ m^{-3}, substantially lower than that of Scenario 2 (see figure 1). In reality the launch $n_{||}$ has to be slightly below the maximum value in order to ensure that no part of the

in these simulations (with some spread in θ due to finite beam width), the most significant error introduced will be that the local RF power, and resultant fast electron, density at the flux surface corresponding to the island location could be underestimated due to the trapping of heated electrons within the magnetic island. Such an increase in local power and fast electron density would lead to a corresponding increase in the importance of non-Maxwellian effects on the wave damping. This effect may in fact be desirable in LHCD localization when RF
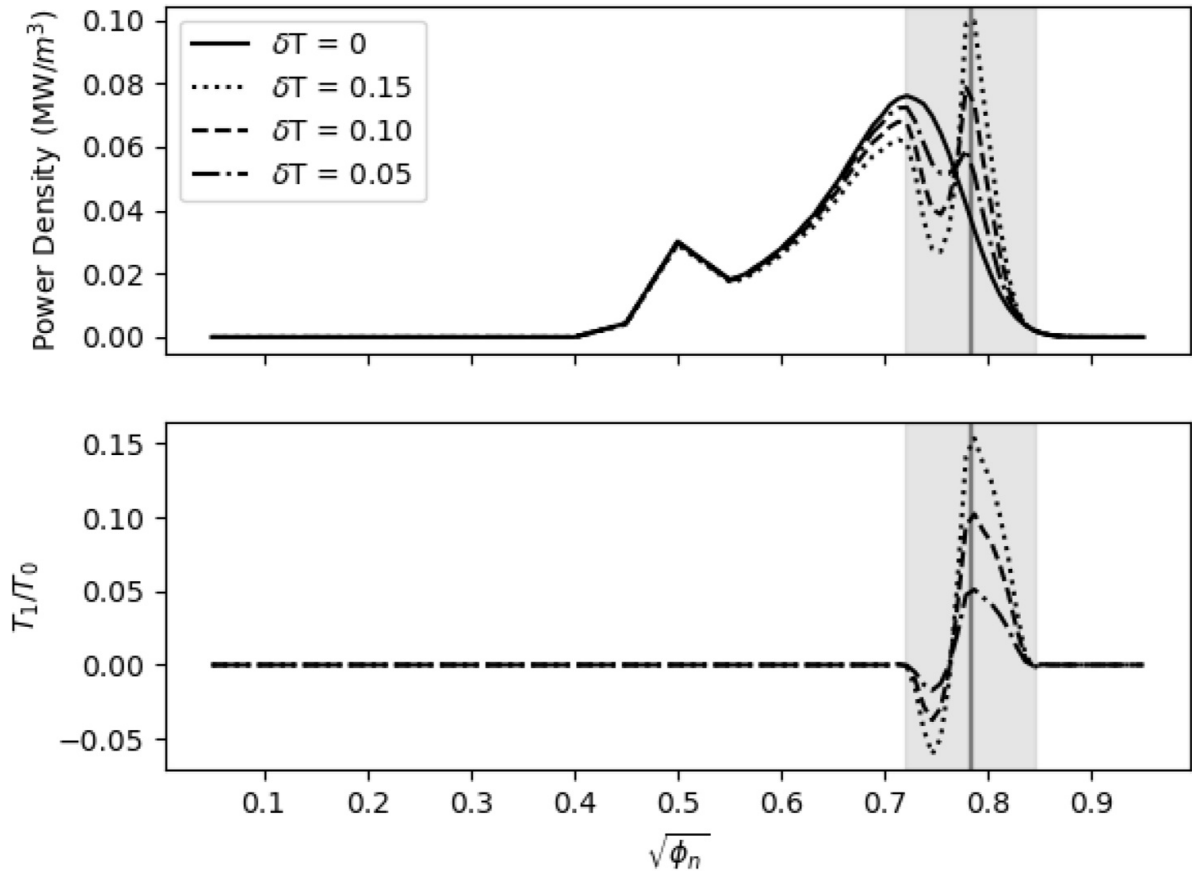
Figure 3. Results of a GENRAY/CQL3D simulation showing the power deposition by the lower hybrid wave and T_1/T_0 vs. the square root of the normalized toroidal magnetic flux for a 20 cm temperature perturbation centered at the q = 2 flux surface. The vertical line represents the location of the q = 2 flux surface in the simulation and the shaded region represents the region subject to the perturbation. In the case of $\delta T = 0.10$ the power deposited inside the perturbation half width increased by a factor of 1.95 to ~ 5 MW and the power density at the center of the perturbation increased by a factor of 2.18.

launch spectrum, which has finite width, is cut off. In order to reach the q = 2 flux surface where the electron temperature is ~ 7 keV the $n_{||}$ value of the LH wave must be greater than $\sim$-2.05 according to equation (2). Thus, on the LFS in Scenario 2, the wave is inaccessible, or only very marginally accessible in the case of a wave launched from slightly below the mid-plane where one may take advantage of a geometric $n_{||}$ upshift as the wave propagates inwards. Accessibility to the q = 1.5 surface is likely impossible with any LFS launcher configuration in Scenario 2. These analytic estimates were confirmed in raytracing/FP simulations which showed significant power reflection and absorption in the pedestal when LFS launch configurations were utilized. By increasing the magnetic field at the launch location, and therefore Ω_e, the accessibility constraint imposed by equation (1) is relaxed allowing wave accessibility at both the q = 2 and q = 1.5 surfaces.

Lower-hybrid waves in the simulations of Scenario 2 were launched at a frequency of 5 GHz from a 0.5 m high waveguide grill positioned 55 degrees above the high-field side midplane with a total launched power 20 MW. Launched power was fixed to 20 MW, a value commonly used in other ITER studies of LHCD [22], in order to minimize the number of parameters which needed to be scanned. For the purposes of studying the

sensitivity to temperature perturbations the input power should be less important than other launcher parameters, however, scanning input power will be very important when temperature feedback effects are included as local power density determines the onset of RF condensation [13].Two-hundred forty total rays were simulated. Rays were launched at 12 different locations along the waveguide grill. At each of these locations, 20 rays were launched with a peak $n_{||}= -1.57$, a spectral width $\Delta n_{||} = 0.06$, and a $(\sin(x)/x)^2$ spectral shape where $x = 2\pi (n_{||} - 0.5\Delta n_{||})/\Delta n_{||}$. The peak $n_{||}$ value chosen found by the following methodology. The value of peak $n_{||}$ value was scanned from $n_{||} = -1.5$, slightly above the accessibility limit defined in equation (1) for a location 60 degrees above the inboard midplane, to $n_{||} = -2$, the minimum value, defined by equation (2), at which the wave should be able to reach the q = 2 flux surface before Landau damping. In addition to the peak $n_{||}$ value the launch location was also scanned between 0 and 60 degrees off relative to the inboard midplane. Results of these scans were down-selected based on which configurations were capable of providing strong localization, i.e. greater than 50% increases in power density, at both the q = 2 and q = 1.5 flux surfaces when perturbations with $\delta T = 0.15$ were imposed. Results meeting these criteria further down-selection to the configuration that provided the
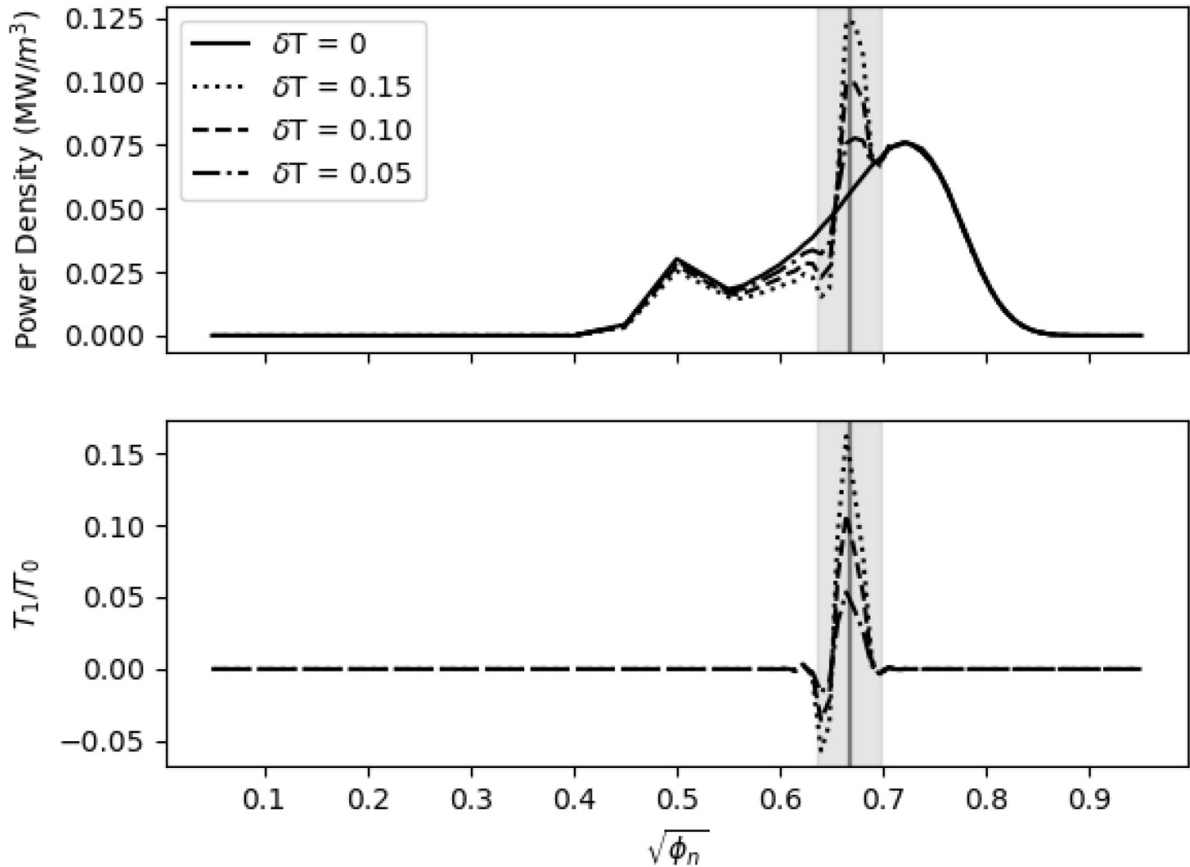
Figure 4. Results of a GENRAY/CQL3D simulation showing the power deposition by the lower hybrid wave and T_1/T_0 vs. the square root of the normalized toroidal magnetic flux for a 10 cm temperature perturbation centered at the q = 1.5 flux surface. The vertical line represents the location of the q = 1.5 flux surface in the simulation and the shaded region represents the region subject to the perturbation.

greatest localization and current drive efficiency. As localization and current drive efficiency both increase with greater v_{ph} this basically amounted to picking the wave with the highest v_{ph} in the range of phase velocities showing strong response to both perturbations. Some launcher configurations were found to achieve stronger localization in response to perturbations at one of the two surfaces but were not found to be able to localize effectively at both. In reactor applications multiple launchers with different spectra could be employed for optimized localization on all flux surfaces vulnerable to instabilities.

The calculated ray trajectories were then used in a CQL3D simulation using 60 flux surfaces. Flux surfaces were packed around in the region where $0.5 \lesssim \sqrt{n} \lesssim 0.9$ in order to increase radial resolution around the rational surfaces of interest without significantly increasing the computational cost of the simulation. Here $\sqrt{n}$ is the square root of normalized toroidal flux. On each flux surface the FP equation was solved with 400 points of resolution in parallel velocity space and 250 points in pitch angle. The FP simulations were evolved over 20 incrementally increasing timesteps starting at $\Delta t = 10 \ \mu s$ and ending $\Delta t = 10$ ms for a total simulated time of 55.55 ms. The fairly long total simulation time used here ensures that the distribution function always comfortably achieves a steady state. This particular CQL3D configuration has been found to ensure very good agreement between launched and damped power. Between 99% and 100% of launched power is damped in these

raytracing/FP simulations over a large range of different parameters (in the baseline, $\delta T = 0$, simulations of Scenario 2 19.957 MW of power was damped).

Smaller numbers of rays were initially used and produced similar results in most cases. However, it was found that the velocity space resolution in the D_{ql} construction in CQL3D became too coarsely grained at low ray number. This coarse graining in velocity-space occasionally led to inconsistent results where very small modifications to the details of the launched spectrum, such as slight changes to where the launch locations along the grill were chosen, led to excessive sensitivity in the simulation results. Increasing the number of total rays in the simulation filled phase space more finely effectively resolving this problem. Moving to large ray number could increase the importance of neglecting effects related to spectral width and interference, however, full-wave simulations of LHCD in ITER have shown full-wave effects to be relatively unimportant in similar regimes [49]. If these effects were truly of concern, however, these reactor relevant scenarios are well suited to the use of the paraxial WKB method, sometimes known as beam-tracing, which could be employed to properly account for them using a code such as Lower Hybrid Beam Tracing (LHBEAM) [50].

Results of the coupled GENRAY/CQL3D simulations of Scenario 2 with 20 cm perturbations on the q = 2 surface are shown in figure 3, and simulations of a 10 cm perturbation on
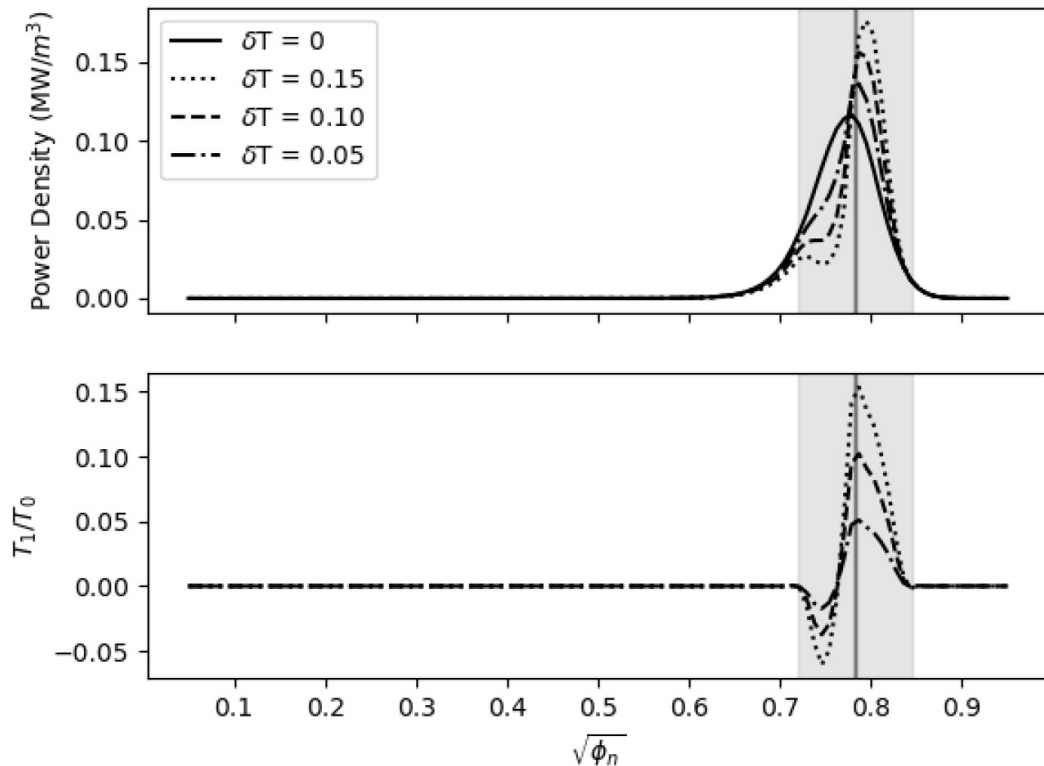
Figure 5. Power deposition with a LHCD launcher configuration optimized for maximum q = 2 power density and power deposition within the perturbation half-width. The LHCD launcher was moved to 60 degrees above the inboard mid-plane and the spectrum centered at $n_{\parallel} = 1.59$. All other simulation parameters are the same as those used in figure 3. After these modifications the majority of the launched 20 MW of LHCD power is deposited within less than half-width of the perturbation when $\delta T \geq 0.1$. Some shadowing is evident in these simulations, but the power deposition remains within the half width and the overall power deposition within the island half width is significantly larger than in simulations optimized for maximization of localization on both the q = 2 and q = 1.5 surfaces.

the q = 1.5 flux surface are shown in figure 4. Localization about the q = 2 and q = 1.5 flux surfaces was obtained in the presence of perturbations at all δT values. With δT values of 0.10 or larger strong localization about the center of the perturbation was obtained. The localization effect was consistent across perturbation widths with localization of power deposition occurring in perturbations with widths of both 10 cm and 20 cm. Substantially better localization, where a majority of the total RF power was deposited within the perturbation half-width, could be achieved when the launcher was optimized for a particular flux surface. An example of such an optimization for localization about the q = 2 flux surface can be seen in figure 5. As ITER has been predicted by Automated System for Transport Analysis (ASTRA) simulations of island stabilization with ECCD to have islands with central δT values in excess of 0.25 at widths > 20 cm [51], these results have promising implications for reactor relevant stability control with LHCD as they indicate that LHCD is indeed sensitive to temperature perturbations, and could be localized to a magnetic island based only on the temperature perturbation in the island. Localization could allow one to stabilize an island well before it induces a disruption.

Finally, the dependence on location of the LH wave damping relative to the location of the temperature perturbation was examined. In order to achieve a high degree of localization without very large temperature perturbations there must already be some quasi-linear damping of the LH wave at the

location where the perturbation is present. If a perturbation is introduced at a location where there is little or no prior LH wave damping, the LH wave damping that results from introducing the perturbation will not be significant unless the perturbation is unrealistically large. For example, in the Scenario 2 simulations when the LHCD launcher was moved to the high-field side midplane the $n_{\parallel}$ evolution experienced by the LH waves while propagating in the toroidal magnetic equilibrium was modified, and as a result the temperature at which the wave damped was increased [44]. After this modification LHCD would no longer localize at the q = 2 flux surface even when a temperature perturbation with δT exceeding 0.2 was imposed (however, localization at the 3–2 flux surface was improved). This condition on localization could reduce the viability of LHCD stabilization schemes in steady state scenarios where the locations of the rational surfaces on which islands form do not necessarily correspond to the locations where the current drive is desired. However, if enhancing the effectiveness of RF stabilization with LHCD is considered in the scenario design phase then it is likely that this problem could be overcome. In some cases, this condition is already satisfied too, for example, in Advanced Reactor Innovation and Evaluation Study Advanced Tokamak (ARIES AT) [21] a 5–2 NTM at the q = 2.5 flux surface was of some concern as it was unclear whether or not the LHCD there would stabilize it. Based on the LHCD profiles presented in the ARIES AT design, it is likely localization by the temperature
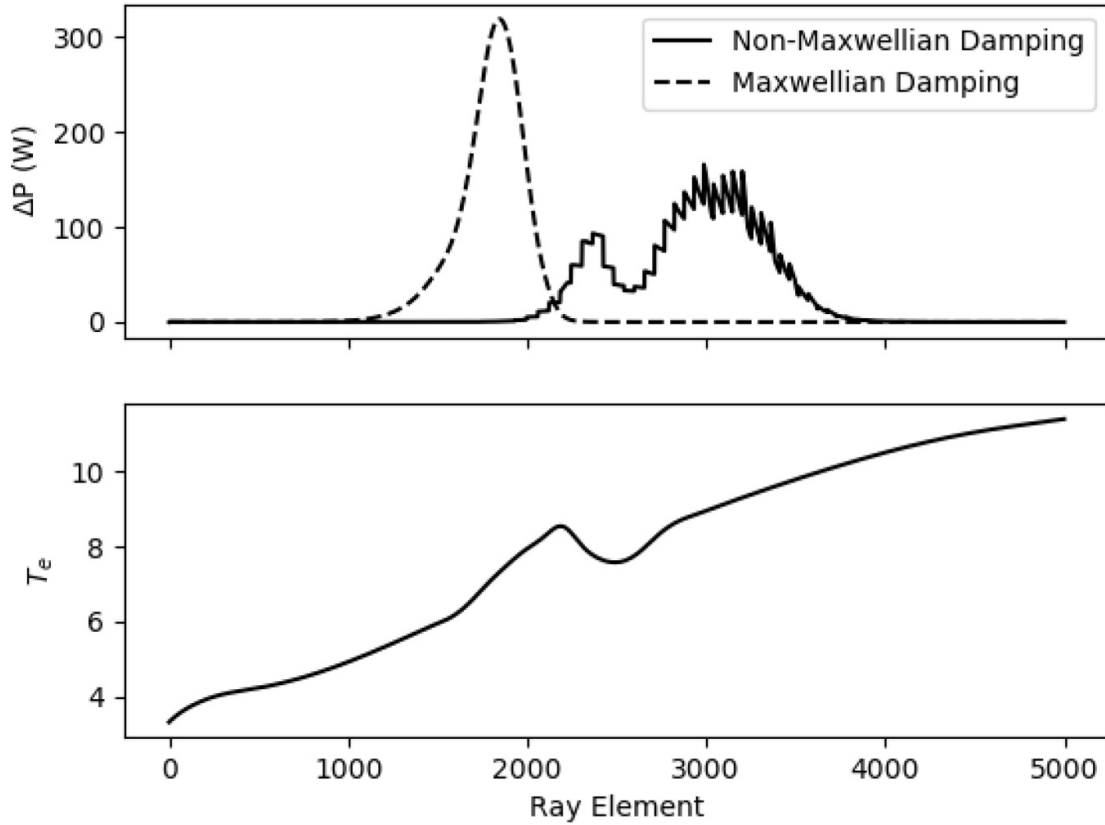
Figure 6. Data from a single ray launched with $n_{||} = -1.58025$ in a GENRAY/CQL3D simulation launched into a perturbed temperature profile with $\delta T = 0.15$. Plotted for Maxwellian and non-Maxwellian wave absorption is the incremental power deposited at each step along the ray ΔP and the temperature T along the ray path vs the distance along the ray. The highest phase velocity rays demonstrated very little quasi-linear response to the perturbation. This suggests that both 3–2 and 2–1 islands could experience localization simultaneously with a broad launch spectrum.

perturbation in the island and further localization by RF condensation would occur making LHCD effective at stabilizing NTMs without the need for additional actuators.

4. The importance of non-Maxwellian effects in RF condensation

In the formulation of RF condensation in [13], the P_{rf} term was dependent on $T(x)$. In reality this dependence is tied to the exact details of the electron distribution function, since the slope of the distribution function, $\partial f_e/\partial v$, can profoundly affect the deposition profile of LHCD. To determine if non-Maxwellian, or quasi-linear, damping was indeed important and should be included in future calculations of RF condensation, the simulations of Scenario 2 were examined. Since the electron distribution function becomes more distorted as the absorbed RF power density increases, if the RF power deposition behavior on an initial island temperature perturbation prior to RF condensation is found to be non-Maxwellian, then the higher power densities expected after localization by RF condensation should also exhibit quasi-linear behavior. To examine the quasi-linear dependence of LH wave damping the simulation data was examined ray by ray. The damping rate on the Maxwellian has been compared to the damping rate of that ray on the electron distribution function after it had

been evolved by the Fokker-Planck equation. The results of this analysis show modification of the damping rate of rays passing through the perturbation as a result of the formation of a Landau plateau. An example of this for a ray with $n_{||} = -1.58025$ can be seen in figure 6.

The formation of a Landau plateau reduces the rays' damping at outer flux surfaces and causes them to penetrate farther into the plasma. This may be a favorable effect since it can prevent 'shadowing' of a magnetic island in some cases. Shadowing occurs when the temperature perturbation in a magnetic island as the result of the RF condensation effect becomes large enough that the wave damps before it is able to reach the center of the island. Non-Maxwellian damping should increase the magnitude of the perturbation required for shadowing to occur. Additionally, it was found that when quasi-linear effects were taken into consideration some of the lowest $n_{||}$ rays demonstrated little response to the temperature perturbations and deposited most of their power further into the plasma. This suggests that it may be possible, with sufficiently broad launched spectrums, to stabilize the 2–1 and 3–2 mode simultaneously. If more accurate island geometry was used in these simulations power densities would be higher as, rather than being spread over the entire volume of the q = 2 flux surface as in the CQL3D simulation where θ symmetry along the magnetic flux surface is assumed, the power and
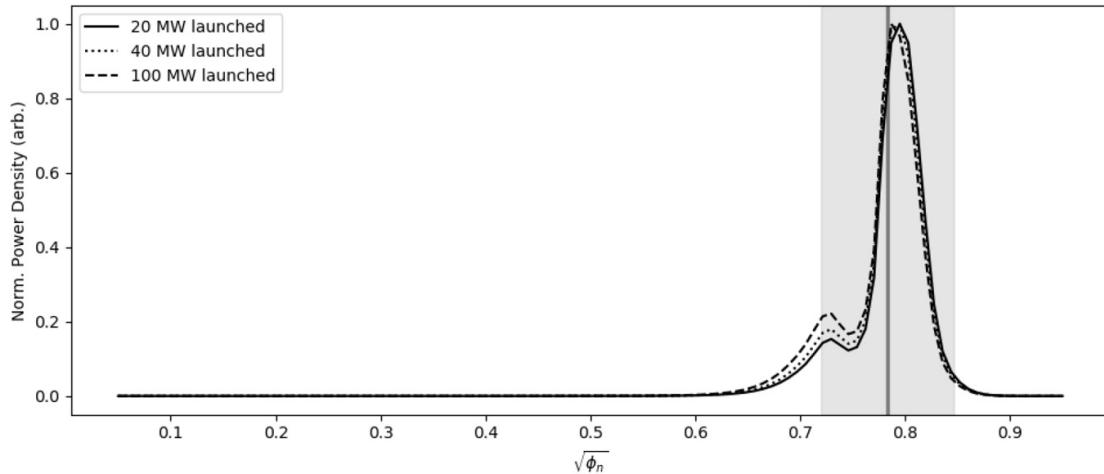
Figure 7. The normalized absorbed RF power density vs square root toroidal flux for temperature perturbation $\delta T = 0.15$ at a number of launched RF powers. This scan was done in order to quantify the effect of increased power and fast electron density on the localization of LHCD about a temperature perturbation. These simulations utilized the same launch configuration as the results presented in figure 5 and were optimized for maximum localization about the q = 2 flux surface. Little change is observed with increases in RF power density, but the small degree of shadowing seen in figure 5 is slightly reduced as RF power density increases. This is a result of increased ray damping length and agrees with prior analytic estimates which predicted decreased shadowing at longer ray damping lengths [52].

some fraction of the driven fast electron population would be localized to a much smaller volume within the magnetic island. The use of a 20 MW launch power in the Scenario 2 simulations offsets this inaccuracy somewhat as stabilization of magnetic islands in a pulsed or hybrid scenario would likely not require 20 MW of RF power. The total launched power density in these use cases would be significantly, perhaps even an order-of-magnitude lower, based on simulations of the stabilization of islands in ITER Scenario 2 using ECCD [51–53], however, even at lower power densities LHCD exhibits quasi-linear behavior. The inclusion of quasi-linear damping could significantly modify the hysteresis effect LH waves experience as they undergo RF condensation. Though, the modification as a result of quasi-linear effects will likely serve to reduce the amount of edge deposition in the magnetic island and improve the relative increase of current at the island O-point this is because the quasi-linear effects observed here tend to increase the power deposition length of the lower-hybrid wave as demonstrated in figure 6. Increasing power deposition length has been shown in analytic studies of the non-linear hysteresis behavior exhibited by waves undergoing RF condensation to, in many cases, actually improve the localization of the wave about the center of magnetic islands by reducing shadowing [54]. While the increased local RF power density and trapped electron density which could occur in an island cannot be modeled here with the available tools, we can study the effect of enhanced non-Maxwellian behavior. This can be done through a relatively simple modification to the calculation in figure 5, where a launcher configuration optimized for the q = 2 island was simulated and a small amount of shadowing was observed. To demonstrate that increased power and fast electron density improves localization the launched power was systematically raised up to 100 MW. The results of these simulations are shown in figure 7. This amount of launched power is obviously unrealistic, but is intended to show that

large increases in power and fast electron density only have a subtle effect on the deposition profiles, and that this change is in fact beneficial. Thus, it is expected that even if there were a large modification to the local RF source term due to increased local power and fast electron density in the island this modification would tend to make the RF condensation effect more robust rather than weaken it.

Since we have shown here the power deposition profile can be significantly modified by non-Maxwellian damping, the evolution of the electron distribution function in response to the RF will need to be included in future simulations of LH waves undergoing RF condensation and simple linear damping calculations will be insufficient. Thus, rather than solving a simplified thermal diffusion equation the full Fokker-Planck equation describing the electron distribution function inside of the island will need to be solved due to the strong quasi-linear dependence of the P_{rf} term.

5. Conclusion

LHCD localization in response to temperature perturbations has been demonstrated in simulations of reactor relevant conditions. For magnetic island-like radial temperature perturbations located at the q = 2 surface with a δT values of 0.10–0.15, which can reasonably occur in magnetic islands resultant from an NTM before RF condensation feedback, strong localization of LH wave absorption occurred for reactor parameters characteristic of ITER Scenario 2. In all simulations of LHCD localization the majority of the LHCD within the perturbation was located within the half-width, and RF power densities in the perturbed region were more than doubled when the perturbation exceeded $\delta T \sim 0.1$. The strong localization observed in these simulations could be sufficient, in some situations, to stabilize a magnetic island without

further localization by RF condensation. Smaller temperature perturbations with δT values of 0.05 exhibited modest localization which could reduce the launched power density required to achieve island stabilization. In these simulations the same launch spectrum was used to localize current drive on both rational surfaces for simplicity. Greater localization can be obtained if the launcher configuration is tailored to induce localization on a specific flux surface or multiple launchers with different configurations are used. Finally, if the LH wave were to induce RF condensation in these cases the localization, and therefore island stabilization efficiency, of the LHCD could be increased further.

The non-linear evolution of the electron distribution function in these simulations showed that the effect of non-Maxwellian damping, not considered in previous RF condensation models [13, 54], must be included for LH waves. Therefore, future simulations of RF condensation of LH waves should calculate the evolution of the electron distribution function in response to the RF to accurately determine the RF power deposition profiles. While these results have been obtained using 1-D radial temperature perturbations, due to the predictable nature of LH wave propagation in the single pass damping regimes present in these simulations, the results can be extrapolated to a more complicated island geometry and will be used in to inform more sophisticated RF condensation models that calculate the non-linear evolution of the LHCD profiles and temperature within a magnetic island. Iteration of raytracing/Fokker-Planck simulations that precisely calculate damping in the island geometry with simulations of the temperature diffusion in the magnetic island should allow one to demonstrate non-Maxwellian RF condensation of LH waves.

It is not unlikely, based on these results, that fully self-consistent simulations with the inclusion of correct magnetic geometry and temperature feedback could produce an even more robust RF localization response. Such simulations could reach higher values of local RF power density due to localization of wave damping within the magnetic island. This will allow the onset of RF condensation at lower launched RF power levels [13]. The magnetic insulation effect observed in islands present in large tokamaks has been sufficient to produce perturbations comparable to the largest, $\delta T = 0.15$, used in this study even *without* direct RF heating of the magnetic island [32] suggesting substantial localization could occur even without further condensation, and it is expected the achievable δT as a result of RF condensation causing positive feedback could exceed the values investigated here. The final concern about the transition of these results to a complete model is the case where an enhanced fast electron density develops within the island as a result of trapping. Greater LHCD produced fast electron density will result in more robust Landau plateau generation and serve to enhance any non-Maxwellian behavior. However, analytic studies of RF condensation suggest that there can be a 'shadowing effect' which under some circumstances reduces penetration into the island by the LH waves [54], and the increased damping length associated with plateau formation can be beneficial under such circumstances. (Additionally, shadowing might be mitigated through pulsing the RF [55].)

It is worthwhile also to note that the advantageous scenarios were achieved using inside launch lower hybrid waves, i.e. from the high field side of the tokamak. The use of inside launch waves has been contemplated for driving toroidal current in tokamaks such as ARC, and CFETR [24, 48]. However, the use of inside-launch waves in a tokamak reactor, particularly when they drive current away from the tokamak center where magnetic islands tend to reside, carries also the possibility of an advantageous, though speculative, synergistic effect [55, 56] of drawing some of the lower hybrid power from the alpha particles through an alpha channeling effect [57, 58].

Even without the further upside associated with inside launch, these results showing strongly localized power deposition already serve to dispel the notion that LHCD is inherently limited to use as broad steady-state current drive actuator and could, with proper scenario and RF system design, be used as localized, high-efficiency, current drive actuator for stability control. Moreover, with careful system design, it is likely that the localization of LHCD and stabilization of NTMs could be achieved nearly passively, i.e. without the need for significant active feedback control. This could have significant implications for the role of LHCD in future fusion experiments and reactors such as CFETR and ARC.

Acknowledgments

References

[1] Gerasimov S.N. *et al* 2018 Overview of disruptions with JET-ILW EXP_P1-24, paper presented at *27th IAEA Int. Conf. on Fusion Energy*, Ahmedabad, India
[2] de Vries P.C. *et al* 2016 *Nucl. Fusion* **56** 026007
[3] Reiman A.H. 1983 *Phys. Fluids* **26** 1338
[4] Fisch N.J. and Boozer A.H. 1980 *Phys. Rev. Lett.* **45** 720
[5] Hegna C.C. and Callen J.D. 1997 *Phys. Plasmas* **4** 2940
[6] Zohm H. 1997 *Phys. Plasmas* **4** 3433
[7] La Haye R.J. 2006 *Phys. Plasmas* **13** 055501
[8] Fisch N.J. 1987 *Rev. Mod. Phys.* **59** 175
[9] Fisch N.J. 1978 *Phys. Rev. Lett.* **41** 873
[10] Karney C.F.F., Fisch N.J. and Jobes F.C. 1985 *Phys. Rev. A* **32** 2554
[11] Warrick C.D. *et al* 2000 *Phys. Rev. Lett.* **85** 574
[12] Prater R. 2004 *Phys. Plasmas* **11** 2349
[13] Reiman A.H. and Fisch N.J. 2018 *Phys. Rev. Lett.* **121** 225001
[14] Karney C.F.F. and Fisch N.J. 1981 *Nucl. Fusion* **21** 1549
[15] Karney C.F.F. and Fisch N.J. 1979 *Phys. Fluids* **22** 1817
[16] Brambilla M. 1976 *Nucl. Fusion* **16** 47
[17] Brambilla M. 1979 *Nucl. Fusion* **19** 1343
[18] Troyon F. and Perkins F.W. 1974 *Proc. of the 2nd Topical Conf. on Radiofrequency Plasma Heating* (Texas Tech University, Lubbock, Texas), Paper B4
[19] Bonoli P.T. 1984 *IEEE Trans. Plasma Sci.* **12** 95

[20] Jardin S.C., Kessel C.E., Bathke C.G., Ehst D.A., Mau T.K., Najmabadi F. and Petrie T.W. The ARIES Team 1997 *Fusion Eng. Des.* **38** 27
[21] Jardin S.C. *et al* 2006 *Fusion Eng. Des.* **80** 25
[22] Decker J. *et al* 2011 *Nucl. Fusion* **51** 073025
[23] Podpaly Y.A., Olynyk G.M., Garrett M.L., Bonoli P.T. and Whyte D.G. 2012 *Fusion Eng. Des.* **87** 215
[24] Sorbom B.N. *et al* 2015 *Fusion Eng. Des.* **100** 378
[25] Cardinali A. *et al* 2017 *Plasma Phys. Control. Fusion* **59** 074002
[26] Ding B.J. *et al* 2018 *Nucl. Fusion* **58** 095003
[27] Cesario R. *et al* 2010 *Nat. Commun.* **1** 55
[28] Luce T.C., Lin-Liu Y.R., Harvey R.W., Giruzzi G., Politzer P.A., Rice B.W., Lohr J.M., Petty C.C. and Prater R. 1999 *Phys. Rev. Lett.* **83** 4550
[29] Zohm H. *et al* 1999 *Nucl. Fusion* **39** 577
[30] Fitzpatrick R. 1995 *Phys. Plasmas* **2** 825
[31] Hazeltine R.D., Helander P. and Catto P.J. 1997 *Phys. Plasmas* **4** 2920
[32] Nave M.F.F., Edwards A.W., Hirsch K., Hugon M., Jacchia A., Lazzaro E., Salzmann H. and Smeulders P. 1992 *Nucl. Fusion* **32** 825
[33] de Vries P.C., Waidmann G., Kramer-Flecken A., Donne A.J.H. and Schuller F.C. 1997 *Plasma Phys. Control. Fusion* **39** 439
[34] Isayama A., Kamada Y., Ozeki T. and Isei N. 1999 *Plasma Phys. Control. Fusion* **41** 35
[35] Inagaki S., Tamura N., Ida K., Nagayama Y., Kawahata K., Sudo S., Morisaki T., Tanaka K. and Tokuzawa T. LHD Experimental Group) 2004 *Phys. Rev. Lett.* **92** 055002
[36] Bardoczi L., Rhodes T.L., Carter T.A., Crocker N.A., Peebles W.A. and Grierson B.A. 2016 *Phys. Plasmas* **23** 052507
[37] Smirnov A.P., Harvey R.W. and Kupfer K. 1994 *Bull Amer. Phys. Soc.* **39** 1626
[38] Harvey R.W. and McCoy M.G. 1993 The CQL3D Fokker-Planck code *Proc. IAEA Technical Meeting on Numerical Modeling of Plasmas* (Montreal, Canada, 1992) (Vienna: IAEA) (https://www.compxco.com/cql3d_manual_150122.pdf)

[39] Petrov Y.V. and Harvey R.W. 2016 *Plasma Phys. Control. Fusion* **58** 115001
[40] Technical Basis for the ITER-FEAT Outline Design 2000 *ITER-EDA Documentation Series IAEA-ITEREDA/DS-19* (Vienna: IAEA) (https://www-pub.iaea.org/MTCD/publications/PDF/ITER-EDA-DS-19.pdf)
[41] Hawryluk R. 1981 An empirical approach to tokamak transport physics of plasmas close to thermonuclear conditions: Proc. of the Course Held in (Varenna, Italy, 27 August–8 September 1979) vol 1, ed B. Coppi (Elsevier) p 1946 (http://w3.pppl.gov/transp).
[42] Hender T.C. *et al* 2007 *Nucl. Fusion* **47** S128
[43] Bellan P.M. and Porkolab M. 1974 *Nucl. Phys. Fluids* **17** 1592
[44] Bonoli P.T. and Ott E. 1982 *Phys. Fluids* **25** 359
[45] Yang C., Bonoli P.T., Shiraiwa S., Ding B., Li M.H., Frank S. and Zhai X. 2018 *Phys. Plasmas* **25** 082516
[46] White R.B., Monticello D.A., Rosenbluth M.N. and Waddell B.V. 1977 *Phys. Fluids* **20** 800
[47] Vahala G., Vahala L. and Bonoli P.T. 1992 *Phys. Fluids* B **4** 4033
[48] Song Y.T. *et al* 2014 *IEEE Trans. Plasma Sci.* **42** 503
[49] Meneghini O. and Shiraiwa S. 2010 *Plasma Fusion Res.* **5** S2081
[50] Bertelli N., Maj O., Poli E., Harvey R., Wright J.C., Bonoli P.T., Phillips C.K., Smirnov A.P., Valeo E. and Wilson J.R. 2012 *Phys Plasmas* **19** 082510
[51] Westerhof E. *et al* 2007 *Nucl. Fusion* **47** 85
[52] La Haye R.J., Ferron J.R., Humphreys D.A., Luce T.C., Petty C.C., Prater R., Strait E.J. and Welander A.S. 2008 *Nucl. Fusion* **48** 054004
[53] La Haye R.J., Isayama A. and Maraschek M. 2009 *Nucl. Fusion* **49** 045005
[54] Rodriguez E., Reiman A.H. and Fisch N.J. 2019 *Phys. Plasmas* **26** 092511
[55] Jin S., Fisch N.J. and Reiman A.H. 2020 *Phys. Plasmas* **27** 062508
[56] Ochs I.E., Bertelli N. and Fisch N.J. 2015 *Phys. Plasma* **22** 082119
[57] Ochs I.E., Bertelli N. and Fisch N.J. 2015 *Phys. Plasma* **22** 112103
[58] Fisch N.J. and Rax J.M. 1992 *Phys. Rev. Lett.* **69** 612